

# Designing Si sphere metagratings: From perfect reflection to large-angle diffraction

Evangelos Almpanis,<sup>1,2</sup> Emmanouil Panagiotidis,<sup>1,2</sup>

Nikolaos Stefanou,<sup>2</sup> and Nikolaos Papanikolaou<sup>1,\*</sup>

<sup>1</sup>*Institute of Nanoscience and Nanotechnology, NCSR “Demokritos,”*

*Patriarchou Gregoriou and Neapoleos Str.,*

*Ag. Paraskevi, GR-153 10 Athens, Greece*

<sup>2</sup>*Section of Condensed Matter Physics,*

*National and Kapodistrian University of Athens,*

*Panepistimioupolis, GR-157 84 Athens, Greece*

## Abstract

A thorough theoretical study of the optical properties of periodic Si nanosphere arrays is undertaken, placing particular emphasis on the synergy between electric and magnetic Mie resonances, which occur in high-refractive-index nanoparticles and can lead to a rich variety of phenomena ranging from perfect reflection to controlled diffraction. By means of systematic calculations using the layer-multiple-scattering method that we properly extended so as to describe periodic arrays with many scatterers per unit cell, in conjunction with finite-element simulations, we optimized surfaces of Si nanospheres that efficiently channel the transmitted light into a single, first-order diffraction beam, following simple design rules based on physical insight. Our results provide compelling evidence that Huygens’ metasurfaces consisting of simple Si nanosphere dimer lattices constitute a promising platform for large-angle unidirectional deflection of transmitted light in the visible, at wavelengths shorter than the diffraction edge of the lattice.

## I. INTRODUCTION

Ultrathin photonic nanostructures, known as metasurfaces, which allow the precise and efficient control of an electromagnetic (EM) wavefront, have recently been proposed and developed<sup>1-4</sup>. Such quasi-two-dimensional (2D) architectures can shape the amplitude, phase, polarization, or even the propagation direction of an EM wave, enabling a variety of practical utilizations such as achromatic lensing<sup>5,6</sup>, planar holography<sup>7-10</sup>, information encryption<sup>11,12</sup>, perfect absorption<sup>13-15</sup>, polarization switching<sup>16-18</sup>, as well as quantum<sup>19</sup> or nonlinear<sup>20,21</sup> photonics.

One of the most intriguing properties of metasurfaces is the steering of incident light to a desired direction. A possible route in achieving beam deflection is by designing surfaces with subwavelength structuring that tailor the phase of a wavefront. The optical response of these, so-called gradient, metasurfaces is described by the generalized Snell's law<sup>22</sup>, where a gradual shift of the transmission or reflection phase from 0 to  $2\pi$  across a particular direction results in anomalous refraction based on the Huygens-Fresnel principle<sup>23-28</sup>. However, when it comes to wide-angle deflection of the light beam, such an approach suffers from fundamental limitations which, together with fabrication difficulties due to complexity, hinder the accomplishment of simultaneous high-efficiency and large-angle light bending<sup>29-31</sup>. A different suggestion based on the equivalence principle<sup>27</sup> was also put forward. The desired field profile in space is achieved through the arrangement of electric and magnetic currents at a common interface which, for visible and infrared light, can be possible by using the induced polarization currents on appropriately designed surfaces<sup>32</sup>. Such designs can also be realized by stacking multilayer metasurfaces with properly engineered reflection and transmission coefficients<sup>33</sup>. An alternative route suggests the development of 2D arrangements of meta-atoms or metamolecules in a periodic lattice, taking advantage of the diffraction properties. Chiefly, such designs, often called metagratings<sup>34</sup>, have the ability to steer light into a particular diffraction channel, reaching remarkable efficiencies even at very high light-bending angles<sup>35-40</sup>. In the transmission configuration, this property would be handy for the realization of almost perfect metalenses<sup>38</sup>.

Obviously, metagrating designs should exhibit low Joule-heating losses together with forward scattering of an incoming EM wave. Both requirements are met when the constituent units are dielectric oligomers that fulfill Kerker's conditions for EM-wave constructive inter-

ference in the far field<sup>41–47</sup>. In this respect, the optical properties of the individual oligomers should be properly combined with the characteristics of the 2D lattice to result in collective resonant modes that can funnel light through a non-zeroth order diffraction channel<sup>37–40</sup>. A distinct feature of dielectric particles is that they support both electric and magnetic resonant modes, which provide unique opportunities to tailor at will the light wavefront. For example, combinations of different optical modes occurring at the same frequency can lead to strong directional scattering<sup>43,45,48</sup>. Though such functional structures of dielectric particles have already been reported<sup>49</sup>, the underlying design principles require a detailed understanding of the complex interaction mechanisms of the photonic modes, which is still missing. So far, the optimum structures were mainly obtained through numerical optimization algorithms, such as neural networks<sup>50</sup>, that do not enable physical insight.

The purpose of the present work is to investigate the possibility to obtain unidirectional deflection of light into large diffraction angles with arrays of Si spheres, in transmission. Pairs of Si spheres have already been shown to exhibit enhanced forward scattering due to constructive interference<sup>43,45,48</sup> and arranging such sphere dimers in a lattice provides additional degrees of freedom to engineer the optical response. Here, we undertake a systematic approach to the design of large-angle diffraction metasurfaces. By means of rigorous, full-electrodynamic, large-scale calculations, we investigate the role of Mie resonances in high-refractive-index spherical particles and pairs of such, their interaction in a lattice, and optimize the properties of so constructed metasurfaces for unidirectional large-angle diffraction of transmitted light. For this purpose, we extend the layer-multiple-scattering (LMS) method<sup>51,52</sup> to deal with different types of scatterers per unit cell, rendering it a powerful tool in the design of complex metasurfaces.

## II. CALCULATIONAL METHOD

The LMS method solves Maxwell’s equations for layered structures of scatterers arranged with the same 2D periodicity in a homogeneous host medium, using spherical-wave expansions around each scattering centre and properly accounting for all multiple-scattering contributions. The global scattering matrix is obtained in a plane-wave basis, through appropriate transformation from spherical to plane waves. This approach is very efficient for problems that involve layers of scatterers with not too large deviations from the spherical

shape<sup>53</sup>. Here we shall briefly describe an extension of the method to treat layers with many scatterers per unit cell.

In an isotropic and homogeneous medium with a relative electric permittivity  $\epsilon$  and magnetic permeability  $\mu$ , the solutions of the electrodynamic equations at given angular frequency  $\omega$  are transverse plane EM waves propagating with wave vector  $\mathbf{q}$  ( $q = \omega\sqrt{\epsilon\mu}/c$ ,  $c$  being the speed of light in vacuum), which have an electric-field component

$$\mathbf{E}_{\mathbf{q}p}(\mathbf{r}) = \text{Re}[\mathbf{E}_0(\mathbf{q}) \exp[i(\mathbf{q} \cdot \mathbf{r} - \omega t)]], \quad (1)$$

with  $\mathbf{E}_0(\mathbf{q}) = E_0 \mathbf{e}_p(\mathbf{q})$ , where  $\mathbf{e}_p(\mathbf{q})$ ,  $p = 1, 2$  denotes the polar and azimuthal unit vectors associated with  $\mathbf{q}$  and defines two independent linear polarization states.

To solve the problem of EM scattering by a single particle, we expand the incident wave into regular at the origin transverse spherical vector wave functions

$$\mathbf{J}_{H\ell m}(\mathbf{r}) = j_\ell(qr) \mathbf{X}_{\ell m}(\mathbf{r}) \quad (2)$$

and

$$\mathbf{J}_{E\ell m}(\mathbf{r}) = \frac{i}{q} \nabla \times j_\ell(qr) \mathbf{X}_{\ell m}(\mathbf{r}) \quad (3)$$

at the given frequency, where  $j_\ell$  are spherical Bessel functions and  $\mathbf{X}_{\ell m}$  vector spherical harmonics defined as

$$\sqrt{\ell(\ell+1)} \mathbf{X}_{\ell m}(\mathbf{r}) = -i \mathbf{r} \times \nabla Y_{\ell m}(\mathbf{r}) \quad (4)$$

with  $Y_{\ell m}(\mathbf{r})$  being the usual spherical harmonics. We similarly define spherical vector functions  $\mathbf{H}_{H\ell m}$  and  $\mathbf{H}_{E\ell m}$ , by replacing in the above Eqs. (2) and (3) the spherical Bessel functions  $j_\ell$  by spherical Hankel functions  $h_\ell^+$ , which are appropriate for outgoing waves. In what follows, we shall employ an index  $L$  to denote, collectively, the indices  $P\ell m$ , where  $P = E, H$ ,  $\ell \geq 1$ , and  $m = -\ell, -\ell + 1, \dots, \ell$ .

In the presence of a scattering particle, the total field is composed of the incoming wave,  $\mathbf{J}_L(\mathbf{r})$ , plus the scattered wave,  $\mathbf{H}_L(\mathbf{r})$ , with appropriate coefficients

$$\mathbf{E}(\mathbf{r}) = \sum_L [a_L^0 \mathbf{J}_L(\mathbf{r}) + a_L^+ \mathbf{H}_L(\mathbf{r})] . \quad (5)$$

The expansion coefficients  $a_L^0$  and  $a_L^+$  are related to each other through the scattering matrix  $\mathbf{t}$  of the individual scatterer. For isotropic spherical particles, this matrix is diagonal in  $L$ ,

with elements  $t_L$  which are independent of  $m$  and can be evaluated analytically. In this case we have  $a_L^\dagger = t_L a_L^0$ .

We now consider a 2D lattice with many particles per unit cell at positions  $\mathbf{R}_{n,\beta} = \mathbf{R}_n + \mathbf{r}_\beta$ , where  $\mathbf{R}_n = n_1 \mathbf{a}_1 + n_2 \mathbf{a}_2$  with  $n_1, n_2$  integer numbers are the Bravais lattice translations and  $\mathbf{r}_\beta$  are appropriate non-primitive vectors within the unit cell. Using the addition theorem for spherical harmonics and Bessel functions, an outgoing spherical wave about a given scatterer can be expanded into incoming spherical waves around a different center through appropriate propagator functions  $\Omega$  at the given frequency, as follows

$$\mathbf{H}_{L'}(\mathbf{r} - \mathbf{R}_{n'\beta'}) = \sum_L \Omega_{LL'}^{n\beta, n'\beta'} \mathbf{J}_L(\mathbf{r} - \mathbf{R}_{n\beta}). \quad (6)$$

Explicit expressions for the propagator functions  $\Omega$  can be found elsewhere<sup>51,54</sup>. Scattering from this array of scatterers, after summing up all multiple-scattering events, can be described through a collective  $T$  matrix given by

$$\mathbf{T} = (\mathbf{t}^{-1} - \mathbf{\Omega})^{-1}, \quad (7)$$

where the  $t$  matrix of individual spherical scatterers is diagonal with matrix elements  $\delta_{\beta\beta'} t_L^\beta$  and

$$\Omega_{\beta L, \beta' L'}(\mathbf{k}_\parallel) = \sum_{n'} \Omega_{LL'}^{n\beta, n'\beta'} \exp[-i\mathbf{k}_\parallel \cdot (\mathbf{R}_n - \mathbf{R}_{n'})] \quad (8)$$

is the 2D Fourier transform of the propagator functions, with  $\mathbf{k}_\parallel$  being the in-plane component of the wave vector  $\mathbf{q}$  reduced within the surface Brillouin zone of the given 2D lattice. The infinite sum in Eq. (8) is efficiently calculated using Kambe's summation method<sup>54</sup>. For a basis of  $N_b$  particles per unit cell and angular momentum cut-off  $\ell_{\max}$ , the matrices in Eq. (7) have dimensions  $2\ell_{\max}(\ell_{\max} + 2)N_b \times 2\ell_{\max}(\ell_{\max} + 2)N_b$ . In the case of submicron spherical particles, the angular momentum expansions involved converge fast. For example, in the calculations carried out in the present work,  $\ell_{\max} = 5$  is sufficient to obtain excellent convergence in all cases studied.

Let the plane wave, described by Eq. (1), be incident on the array of spheres. We can always write the in-plane component of its wave vector as  $\mathbf{q}_\parallel = \mathbf{k}_\parallel + \mathbf{g}'$ , where the reduced wave vector  $\mathbf{k}_\parallel$  lies in the surface Brillouin zone and remains invariant in the (multiple) scattering process due to the periodicity of the structure, and  $\mathbf{g}'$  is a certain reciprocal-lattice vector. In turn, the scattered field at the given frequency has the form of plane waves

propagating or decaying in the positive (+) and negative (-)  $z$  direction, with wave vectors

$$\mathbf{K}_{\mathbf{g}}^{\pm} = (\mathbf{k}_{\parallel} + \mathbf{g}, \pm[q^2 - (\mathbf{k}_{\parallel} + \mathbf{g})^2]^{1/2}), \quad (9)$$

where  $\mathbf{g}$  are vectors of the reciprocal lattice, which correspond to the different diffracted beams.

The transmission and reflection coefficients of the array of scatterers, in the specific plane-wave basis, are obtained using the collective  $T$  matrix defined in Eq. (7) by<sup>51,52,54</sup>

$$S_{sp\mathbf{g},s'p'\mathbf{g}'} = \delta_{ss'}\delta_{pp'}\delta_{\mathbf{g}\mathbf{g}'} + \sum_{\beta\mathbf{L}} \sum_{\beta'\mathbf{L}'} \Delta_{sp\mathbf{g}}^{\beta\mathbf{L}} T_{\beta\mathbf{L},\beta'\mathbf{L}'} A_{\beta'\mathbf{L}'}^{s'p'\mathbf{g}'}, \quad (10)$$

where  $s, s' = \pm$  and

$$A_{\beta H\ell m}^{sp\mathbf{g}} = 4\pi i^{\ell} (-1)^{m+1} \exp(i\mathbf{K}_{\mathbf{g}}^s \cdot \mathbf{r}_{\beta}) \mathbf{X}_{\ell-m}(\mathbf{K}_{\mathbf{g}}^s) \cdot \mathbf{e}_p(\mathbf{K}_{\mathbf{g}}^s) \quad (11)$$

$$A_{\beta E\ell m}^{sp\mathbf{g}} = 4\pi i^{\ell} (-1)^{m+1} \exp(i\mathbf{K}_{\mathbf{g}}^s \cdot \mathbf{r}_{\beta}) [\mathbf{X}_{\ell-m}(\mathbf{K}_{\mathbf{g}}^s) \times \mathbf{K}_{\mathbf{g}}^s] \cdot \mathbf{e}_p(\mathbf{K}_{\mathbf{g}}^s) \quad (12)$$

$$\Delta_{sp\mathbf{g}}^{\beta H\ell m} = \frac{2\pi(-i)^{\ell}}{qA_0K_{\mathbf{g};z}^+} \exp(-i\mathbf{K}_{\mathbf{g}}^s \cdot \mathbf{r}_{\beta}) \mathbf{X}_{\ell m}(\mathbf{K}_{\mathbf{g}}^s) \cdot \mathbf{e}_p(\mathbf{K}_{\mathbf{g}}^s) \quad (13)$$

$$\Delta_{sp\mathbf{g}}^{\beta E\ell m} = \frac{2\pi(-i)^{\ell}}{q^2A_0K_{\mathbf{g};z}^+} \exp(-i\mathbf{K}_{\mathbf{g}}^s \cdot \mathbf{r}_{\beta}) [\mathbf{X}_{\ell m}(\mathbf{K}_{\mathbf{g}}^s) \times \mathbf{K}_{\mathbf{g}}^s] \cdot \mathbf{e}_p(\mathbf{K}_{\mathbf{g}}^s) \quad (14)$$

with  $A_0$  being the surface of the unit cell.

For a plane wave incident on the array of scatterers, say, along the positive  $z$  direction with wave vector  $\mathbf{K}_{\mathbf{g}'}^+$  and polarization  $p'$ , the total transmittance and reflectance are given by

$$\mathcal{T} = \sum_{p\mathbf{g}} |S_{+p\mathbf{g},+p'\mathbf{g}'}|^2 \frac{K_{\mathbf{g}z}^+}{K_{\mathbf{g}'z}^+} \quad (15)$$

and

$$\mathcal{R} = \sum_{p\mathbf{g}} |S_{-p\mathbf{g},+p'\mathbf{g}'}|^2 \frac{K_{\mathbf{g}z}^+}{K_{\mathbf{g}'z}^+}, \quad (16)$$

respectively, while the absorbance is calculated by requiring energy conservation,  $\mathcal{A} = 1 - \mathcal{T} - \mathcal{R}$ . We note in passing that it is straightforward to generalize the LMS method to deal with multiple layers of 2D arrays with many scatterers per unit cell, provided that they have

the same periodicity<sup>51,52</sup>. This method is accurate, rapidly converging, and ideally suited for arrays of spheres. One of its considerable advantages is that it allows to directly access the character of the optical modes of the individual particles (dipolar, quadrupolar, octapolar, etc.) and gain physical insight on the formation of collective modes when these particles are arranged in a lattice.

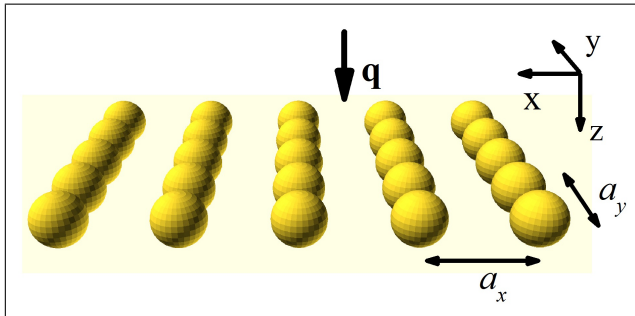


FIG. 1: Schematic of an array of spheres in a rectangular lattice with lattice constants  $a_x$ ,  $a_y$  in the  $x$  and  $y$  direction, respectively.

### III. RESULTS AND DISCUSSION

In dielectric particles, the existence of electric- as well as magnetic-type Mie resonances have attracted considerable attention<sup>45,55–57</sup> because their proper combination can lead to constructive or destructive interference and directional scattering<sup>47,48,58</sup>. In arrays of such particles, multiple-scattering effects may also be significant and are sometimes discussed in terms of interaction between Mie modes<sup>59</sup>. For example, a square array of Si spheres can be designed as a total reflector at wavelengths close to the Mie resonances<sup>60</sup>. In many studies of periodic arrays, the discussion is focused on wavelengths above the lattice diffraction edge, where only a single specular beam exists and the optical response can be related to the complex transmission and reflection coefficients of zeroth order, or to the impedance and effective optical constants<sup>3</sup>. At wavelengths below the diffraction edge, optical power is generally distributed in the different diffraction orders. By manipulating the hybridization between Mie modes, it is possible to control the intensity of light in each diffracted beam. There are several proposals for reflection metagratings<sup>61,62</sup> and recent efforts to develop design rules for such architectures came to the conclusion that anisotropic unit cells supporting at least four resonances are required to achieve control of the wavefront and high efficiency<sup>40</sup>.

For transmission gratings,<sup>33,63,64</sup> one approach is to block the specular transmission and employ asymmetric unit cells to funnel all optical power in a given diffraction order. In the following, we will discuss an implementation of this strategy using lattices of Si spherical particles.

### A. Mie modes and diffraction

First we consider square arrays of Si spheres of the same radius,  $r_1 = 120$  nm, in air, as schematically shown in Fig. 1. In our calculations we use optical constants fitted to the measured data for crystalline Si<sup>65</sup>. The transmission, reflection and absorption spectra for a lattice constant  $a_{x,y} = 400$  nm are shown in Fig. 2(a). The displayed spectra are dominated by two pronounced reflection peaks, the dipolar magnetic (DM) close to 850 nm and the dipolar electric (DE) about 700 nm, which are slightly blue-shifted from the positions of the corresponding Mie resonances of the isolated sphere<sup>66</sup>. By reducing the lattice constant to  $a_{x,y} = 300$  nm, these peaks broaden due to the increased interparticle coupling and merge into each other forming a broad, strongly reflecting band ranging from 700 to 800 nm, as can be seen in Fig. 2(b). The phase acquired by the electric field upon reflection, inside the reflection band, varies with the wavelength according to the character of the Mie resonances. This is clearly visible in the electric field profiles at the two edges of this reflection band, depicted in Figs. 2(c), (d). It is worth-noting that the spectra calculated by the LMS method [lines in Fig. 2(b)] agree very well with the results obtained at increased computational cost using the the finite-element method as implemented in the COMSOL Multiphysics software package [circles in Fig. 2(b)] .

The role of the lattice in the formation of a reflection band can be further elucidated by arranging the Si spheres in a rectangular array with  $a_x = 700$  nm, and  $a_y = 300$  nm (see Fig. 1), where at normal incidence we expect the emergence of diffracted beams in the  $x$  direction for  $\lambda < 700$  nm. In general, the diffraction angle for a particular diffraction order  $m_i$  along the direction with period  $a_i$ , ( $i = x, y$ ) at wavelength  $\lambda$  is given by

$$\varphi_{m_i} = \arcsin(m_i \lambda / a_i n) \tag{17}$$

with  $n$  being the refractive index of the embedding medium.

The reflection spectra for normally incident light, polarized along the long-period axis  $x$



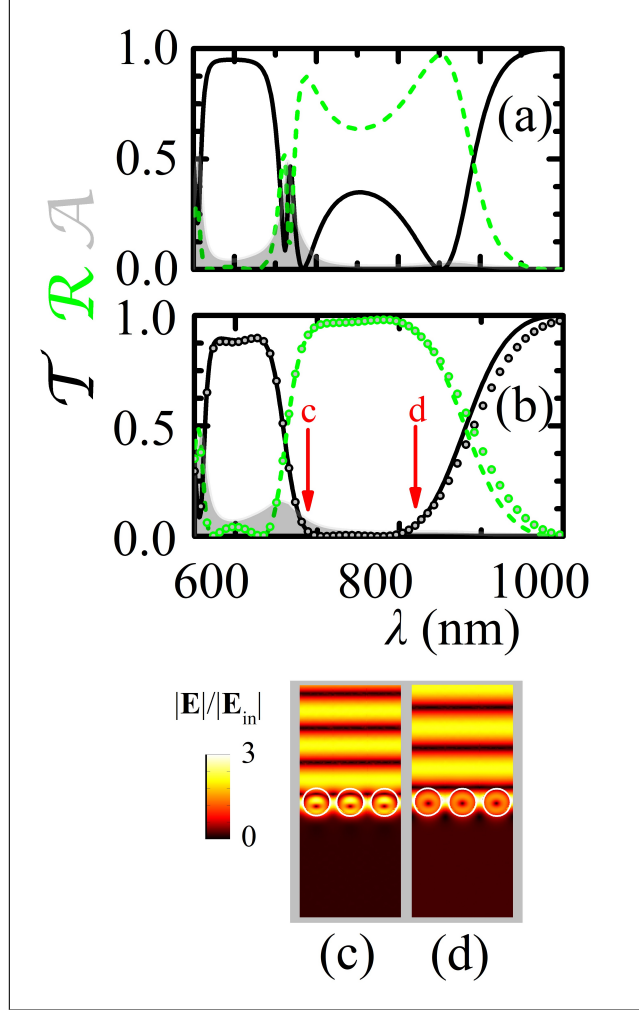


FIG. 2: (a): Optical spectra of a square array (lattice constant  $a_{x,y} = 400$  nm) of Si spheres (radius  $r_1 = 120$  nm) in air, illuminated by normally incident light (see Fig. 1). The transmittance,  $\mathcal{T}$ , reflectance,  $\mathcal{R}$ , and absorbance,  $\mathcal{A}$ , are displayed by solid black lines, dashed green lines, and gray-shaded areas, respectively. (b): The same as in (a), for  $a_{x,y} = 300$  nm. The circles show the results of finite-element calculations using the COMSOL Multiphysics software package. The normalized field profiles at the wavelengths indicated by the arrows in (b) are shown in (c) and (d).

(x-pol) and along the short-period axis  $y$  (y-pol), are shown in Fig. 3(a) and (b), respectively. For  $x$ -polarized light, the DM Mie mode is responsible for the strong reflection peak at longer wavelengths, close to  $\lambda = 920$  nm (dash-dotted green lines), while a sharper and smaller peak associated with the DE mode appears very close to the diffraction edge at 700 nm. The Mie modes can be traced clearly in the specular transmission component,  $\mathcal{T}_0$ , which is useful for wavelengths below the diffraction edge where the intensity of light distributed in the

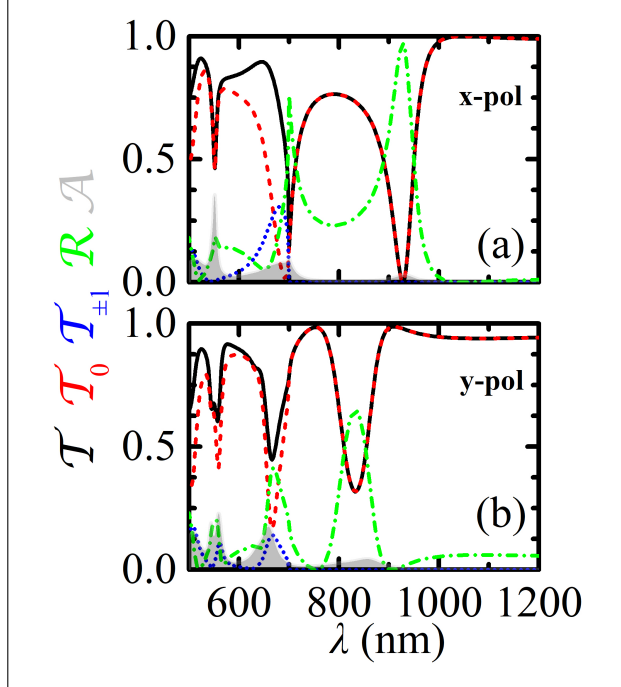


FIG. 3: Reflectance,  $\mathcal{R}$  (dash-dotted green lines), absorbance,  $\mathcal{A}$  (gray-shaded areas), total transmittance,  $\mathcal{T}$  (solid black lines), specular transmittance,  $\mathcal{T}_0$  (dashed red lines), and first-order diffracted transmittance along the  $x$  direction,  $\mathcal{T}_{\pm 1}$  (dotted blue lines) of an array of Si spheres of radius  $r_1 = 120$  nm, arranged on a rectangular lattice with  $a_x = 700$  nm and  $a_y = 300$  nm (see Fig. 1). Light is incident normally with (a):  $x$  polarization and (b):  $y$  polarization.

diffraction channels in the  $x$  direction,  $\mathcal{T}_{\pm 1}$ , becomes significant and the total transmission and reflection spectra are harder to interpret. For  $y$ -polarized light, the Mie modes give weaker reflection peaks. The DM Mie resonance peak is found to be blue-shifted compared to the  $x$ -polarized spectra, while the DE modes cause a significant drop in  $\mathcal{T}_0$ , similar to the spectra for the  $x$  polarization.

By further increasing the long lattice constant,  $a_x$ , the DM Mie modes also move below the diffraction edge. Relevant optical spectra for Si spheres of the same radius,  $r_1 = 120$  nm, arranged on a lattice with  $a_x = 1000$  nm and  $a_y = 300$  nm, are depicted in Fig. 4 for both polarizations. For  $x$ -polarization [see Fig. 4 (a)], the specular transmission,  $\mathcal{T}_0$ , is suppressed at the positions of the Mie resonances, close to 880 nm for the DM mode and 680 nm for the DE mode, with the effect being stronger for the DM mode, while the first-order diffracted light along  $x$ ,  $\mathcal{T}_{\pm 1}$ , is enhanced at these frequencies. The spectra exhibit similar features also for  $y$ -polarized light, the only difference being that the  $\mathcal{T}_0$  minima are now close to

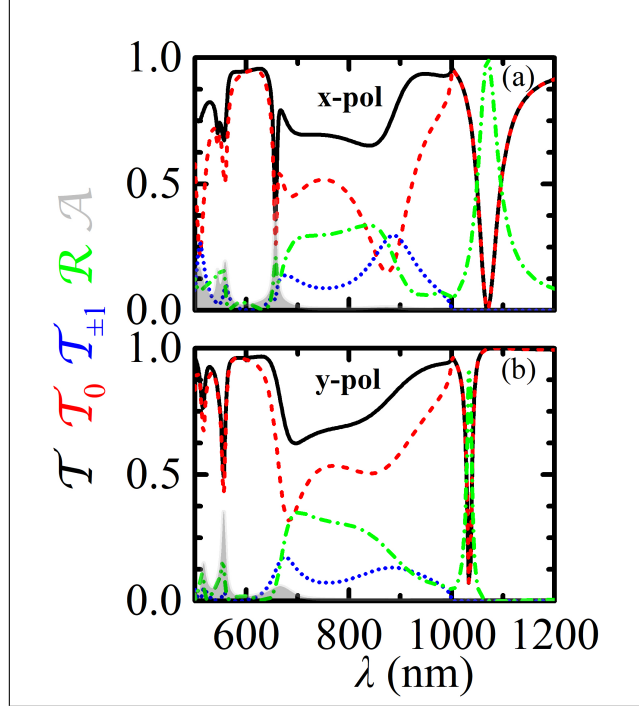


FIG. 4: The same as in Fig. 3, for  $a_x = 1000$  nm and  $a_y = 300$  nm (see Fig. 1).

the DE resonance. Due to the symmetry of the structure, diffraction is equally distributed in the  $m_x = \pm 1$  channels. We note that reflection is not very high in the spectral region between the DM and DE Mie resonances, but a narrow total reflection band is present above the diffraction edge, close to  $\lambda = 1050$  nm. This is ascribed to a mode strongly localized in the sphere rows, which has the characteristics of a leaky slab mode that couples to the continuum and can also lead to a strong reflection band<sup>67</sup>. These latter modes, which appear only above the diffraction edge, are not related to a particular Mie resonance and can be shifted to longer wavelengths simply by increasing  $a_x$ .

To summarize, we have shown that, in simple 2D arrays of Si spheres, the presence of Mie resonances can lead to destructive interference in the specular transmission channel. Moreover, at wavelengths where diffraction takes place, the layers can be highly transmissive at the Mie resonances but light escapes through the higher-order diffraction channels.

## B. A Si sphere dimer

The scattering properties of dielectric dimers and multiparticle clusters with overlapping electric and magnetic Mie resonances (Kerker's condition) have drawn significant attention

and several realizations were considered, since constructive interference results in enhanced forward scattering<sup>45</sup>.

The scattering cross section of an isolated pair of Si spheres<sup>43,47,48</sup> with radii  $r_1 = 120$  nm and  $r_2 = 80$  nm, separated by a 10 nm air gap, calculated using the COMSOL Multiphysics software package, is shown in Fig. 5(a). The radii were chosen so that the DM mode of the smaller sphere is in the same spectral region as the DE mode of the larger sphere. Mode overlap leads to enhanced forward scattering at wavelengths around 650 nm as shown in the far field plots [Fig. 5(b)], while the asymmetry of the dimer deflects light towards the direction of the larger sphere. The structure can be optimized to reduce backscattering by tilting the dimer by an angle  $\theta = 28^\circ$  around the center of the larger sphere. As shown with the dashed red lines in Fig. 5(b), this tilted configuration leads to stronger forward scattering and larger deflection angle while the scattering cross section spectrum changes only slightly (not shown). This suppression of backscattering is accompanied by hot-spots of the electric field in the region between the spheres<sup>58</sup>.

### C. Surfaces for efficient large-angle deflection of light

Dielectric oligomers with controlled, directional, scattering as the simple Si sphere dimer considered here are interesting building blocks of periodic metagratings, which efficiently deflect light towards the direction of a particular diffraction order<sup>5,36,40</sup>.

To understand the different underlying mechanisms, we replace the single Si spheres in the rectangular lattice considered previously (see Fig. 3) with the asymmetric Si sphere dimer  $r_1 = 120$  nm,  $r_2 = 80$  nm, discussed above. The geometry is schematically shown in Fig. 6(a) and corresponding transmission spectra for the different diffraction orders, for light incident normally and polarized along the  $x$  direction, are depicted in Fig. 6(b). These spectra should be compared with those of the lattice with the single spheres, for the same polarization, depicted in Fig. 3(a). It can be seen that the sharp drop in the transmission just above 900 nm due to the DM mode of the larger spheres is preserved also in the dimer lattice. The Mie resonances of the smaller spheres affect the spectra below 700 nm, but the characteristic drop of the specular transmittance,  $\mathcal{T}_0$ , just below 700 nm, attributed to the DE mode of the larger sphere, appears in the spectra of both geometries. Additionally, the first-order diffracted beams in the  $x$  direction ( $m_x = \pm 1$ ) now become asymmetric. More

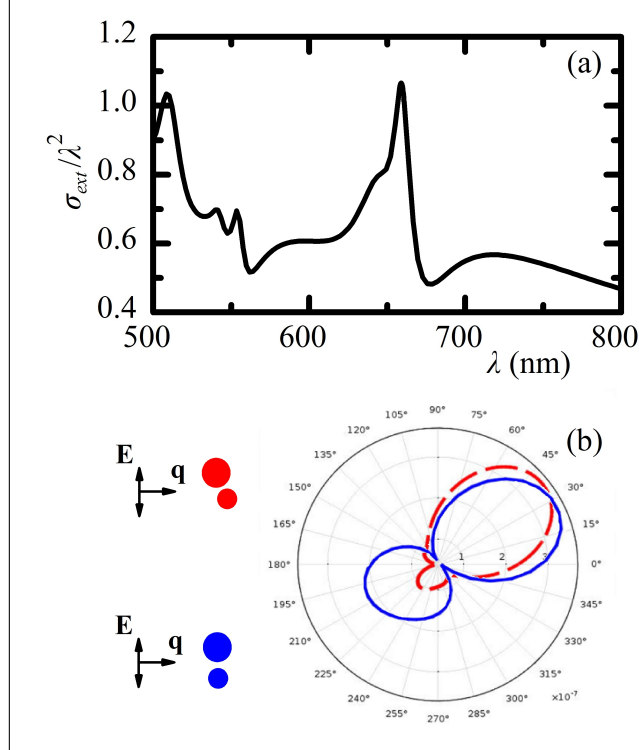


FIG. 5: (a): Normalized extinction cross section,  $\sigma_{\text{ext}}$ , of a Si sphere dimer with radii  $r_1 = 120$  nm and  $r_2 = 80$  nm, separated by 10 nm, for light incident normally to (and polarized along) the dimer axis. (b): Far-field plots at  $\lambda = 650$  nm, for the geometries shown on the left: Light incident normally and polarized along the dimer axis (solid blue line); light incident on a dimer tilted by  $28^\circ$  around the center of the larger sphere, where forward scattering and deflection angle are maximized (dashed red line).

power is directed in the  $\mathcal{T}_{+1}$  beam and light is bent in the direction of the larger spheres, which is consistent with the scattering pattern of the isolated pair [see Fig. 5(b)]. Higher-order diffraction ( $|m_x| > 1$ ) is negligible in the spectral window considered. A strongly localized leaky mode just below  $\lambda = 800$  nm, which yields a sharp transmission dip, is also worth-mentioning. The existence of such Fano-type modes has been discussed in the literature<sup>68,69</sup>, and their position and strength depends on their interaction with the Mie modes of the spheres.

The most interesting spectral region for our purposes appears below the diffraction edge, at  $\lambda$  ranging from 650 nm to 700 nm, where the interaction of the DE Mie modes of the larger spheres strongly suppresses the specular transmission but, at the same time, the spectral

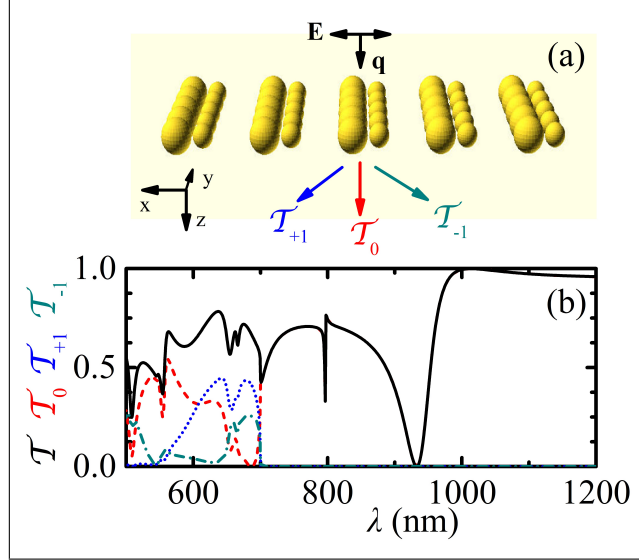


FIG. 6: (a): An array of Si sphere dimers with radii  $r_1 = 120$  nm and  $r_2 = 80$  nm, with their centers on the same plane and a separation of 10 nm along the  $x$  direction, arranged in a rectangular lattice with  $a_x = 700$  nm and  $a_y = 300$  nm. (b): Transmittance of the structure described in (a) for normally incident  $x$ -polarized light. Solid black line: Total transmittance,  $\mathcal{T}$ . Dashed red line: Transmittance through zeroth-order diffraction,  $\mathcal{T}_0$  (specular transmittance). Dotted blue line: Transmittance in the  $m_x = +1$  diffraction channel,  $\mathcal{T}_{+1}$ . Dash-dotted green line: Transmittance in the  $m_x = -1$  diffraction channel,  $\mathcal{T}_{-1}$ .

overlap of the DE and DM modes of the different spheres (Kerker's condition) minimizes the reflectance. As a result, most of the power is transmitted through the first-order diffraction channels. The asymmetry between the first-order diffraction channels in the  $x$  direction,  $\mathcal{T}_{+1}$  and  $\mathcal{T}_{-1}$ , is not large but can be further optimized given the far-field scattering amplitude of the isolated Si pair [see Fig. 5(b)].

Let us consider a rectangular array, with lattice parameters  $a_x = 670$  nm and  $a_y = 270$  nm, with the Si dimers rotated by an angle  $\theta = 28^\circ$  about an axis parallel to the  $y$  direction passing through the centre of the larger spheres, as shown in Fig. 7(a). This structure is optimized for maximum intensity of directional transmission and larger deflection angle, through extensive numerical calculations by the LMS method. The relevant transmission spectra associated with the different diffracted beams are displayed in Fig. 7(b). Transmission towards the larger sphere is maximized while leakage of light in all other channels is minimized at wavelengths about 660 nm and  $\mathcal{T}_{+1}$  reaches a peak close to 70% while the

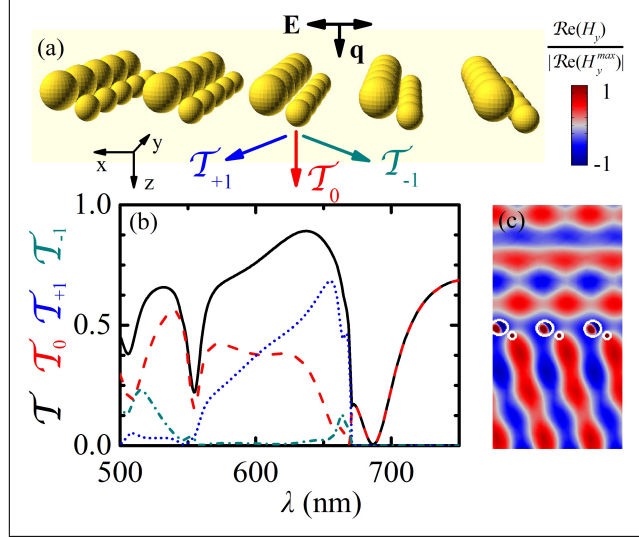


FIG. 7: (a): A rectangular array, with  $a_x = 670$  nm and  $a_y = 270$  nm, of the Si sphere dimers of Fig. 6(a) rotated by an angle  $\theta = 28^\circ$  about an axis parallel to the  $y$  direction passing through the centers of the larger spheres. (b): Transmittance of the structure described in (a) for normally incident  $x$ -polarized light. Solid black line: Total transmittance,  $\mathcal{T}$ . Dashed red line: Transmittance through zeroth-order diffraction,  $\mathcal{T}_0$  (specular transmittance). Dotted blue line: Transmittance in the  $m_x = +1$  diffraction channel,  $\mathcal{T}_{+1}$ . Dash-dotted green line: Transmittance in the  $m_x = -1$  diffraction channel,  $\mathcal{T}_{-1}$ . (c) Profile of the  $y$  component of the magnetic field,  $H_y$ , in an  $x$ - $z$  plane passing through the centers of the spheres, at  $\lambda = 650$  nm.

bending angle at  $\lambda = 650$  nm is  $\varphi_{+1} = 76^\circ$ . The calculated magnetic-field profile at this wavelength is shown in Fig. 7(c). Interestingly, strong diffraction persists with more than 50% of the incoming power funneled in the  $m_x = +1$  channel in a relatively broad spectral window ranging from about 630 nm to 670 nm.

A comment on the necessity of a full multipole description of the effects discussed here above is relevant. As mentioned previously, all higher multipoles are included in our calculations and the results reported in the present work are fully converged. On the other hand, dipole models are often used and assumed sufficient<sup>46</sup> to describe the optical response of isolated Si dimers of similar size noting that quadrupole modes, though they result in strongly anisotropic scattering, have longer lifetimes and thus exhibit higher losses compared to the dipole modes. The influence of the different multipoles on the results for the structures studied here is shown in Fig. 8, where we present spectra calculated for our optimized Si sphere

dimer structure of Fig. 7(a) by truncating the multipole expansions involved at  $\ell_{\max} = 1$  and  $\ell_{\max} = 2$ . It can be seen that, qualitatively, the overall behavior of the system can be described by the dipole approximation since both the suppression of the specular transmission and the strong asymmetry of the first-order diffraction channels are reproduced. However, quantitative information requires to include quadrupole ( $\ell = 2$ ) terms while  $\ell > 2$  give only small contributions and can be ignored.

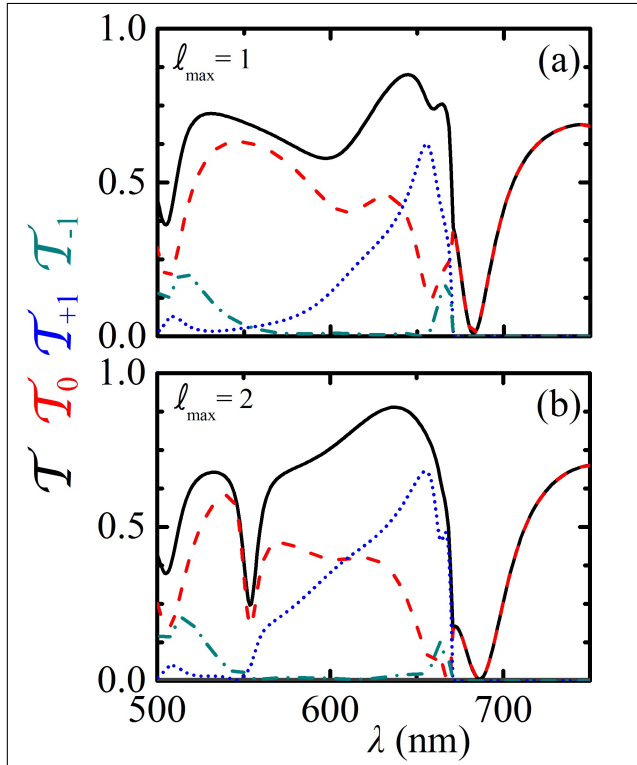


FIG. 8: The spectra of Fig. 7(b), calculated by taking into account (a): Only dipolar terms ( $\ell_{\max} = 1$ ). (b): Dipolar and quadrupolar terms ( $\ell_{\max} = 2$ ).

Our structures achieve strong and efficient light bending and compare very well to other metasurfaces proposed for this purpose, as can be seen in Table I, where  $\mathcal{T}_{\max}$  and  $\eta$  are the maximum transmittance and light-deflection angle obtained. The present design is simple, optimization was based on physical insight, and similar principles can be used to design efficient deflectors at different wavelengths by appropriately adjusting the material and geometrical parameters involved. Although we used air as embedding medium for our proof of principle design, following the same optimization procedure, similar efficiencies can be obtained in glass, at somewhat longer wavelengths in the near infrared.



TABLE I: Comparative performance of different designs of transmissive metasurfaces for large-angle unidirectional deflection of light.

Ref.	$\eta$	$\mathcal{T}_{\max}$	Frequency	Complexity
40	70°	95%	mid-infra	multi-parametric
37	75°	84%	near-infra	extremely complex
39	80°	50%	visible	very complex
39	55°	90%	visible	very complex
38	82°	50%	visible	Si-cylinder dimer
This work	76°	70%	visible	Si-sphere dimer in air

#### IV. CONCLUSION

In summary, we developed a strategy to engineer metasurfaces capable of strongly and efficiently deflecting polarized transmitted light. This consists in first designing a periodic array of high-refractive-index nanoparticles that block the forward transmission channel and, subsequently, add a second smaller particle per unit cell in order to guide light asymmetrically through constructive interference to the desired diffraction order. Our approach takes advantage of the simultaneous existence of DM and DE resonant modes in such particles, and the deflection angle can be maximized by adjusting the geometric parameters involved to tune interference effects close to the diffraction edge of the lattice. The efficiency of this strategy was demonstrated on simple periodic arrays of asymmetric Si sphere dimers where, by means of systematic numerical calculations using an extension of the LMS method in conjunction with finite-element simulations, we provided unambiguous evidence for large-angle unidirectional deflection of visible light. The underlying design principles, which are based on the interaction between DM and DE Mie resonances, can be applied to other similar systems such as cylinders on a substrate and establish simple rules for facile optimization of surfaces of arrays of nanoparticles based on the scattering properties of the individual building units.

## V. FUNDING INFORMATION

We acknowledge support of this work by the project Development of Materials and Devices for Industrial, Health, Environmental and Cultural Applications (MIS 5002567) which is implemented under the Action for the Strategic Development on the Research and Technological Sector, funded by the Operational Program "Competitiveness, Entrepreneurship and Innovation" (NSRF 2014-2020) and co-financed by Greece and the European Union (European Regional Development Fund). E. A. was supported by the General Secretariat for Research and Technology and the Hellenic Foundation for Research and Innovation under Grant 1819. E. P. acknowledges support from IKY PhD scholarship.

---

\* Electronic address: n.papanikolaou@inn.demokritos.gr

<sup>1</sup> N. Yu and F. Capasso, "Flat optics with designer metasurfaces," *Nat. mater.* **13**, 139-150 (2014).

<sup>2</sup> A. V. Kildishev, A. Boltasseva, and V. M. Shalaev, "Planar photonics with metasurfaces," *Science* **339**, 1232009 (2013).

<sup>3</sup> A. E. Minovich, A. E. Miroshnichenko, A. Y. Bykov, T. V. Murzina, D. N. Neshev, and Y. S. Kivshar, "Functional and nonlinear optical metasurfaces," *Laser Photon. Rev.* **9**, 195-213 (2015).

<sup>4</sup> A. A. High, R. C. Devlin, A. Dibos, M. Polking, D. S. Wild, J. Perczel, N. P. de Leon, M. D. Lukin, and H. Park, "Visible-frequency hyperbolic metasurface," *Nature* **522**, 192-196 (2015).

<sup>5</sup> M. L. Tseng, H. Hsiao, C. H. Chu, M. K. Chen, G. S. A. Liu, and D. P. Tsai, "Metalenses: Advances and applications," *Adv. Opt. Mater.* **6**, 1800554 (2018).

<sup>6</sup> W. T. Chen, A. Y. Zhu, J. Sisler, Z. Bharwani, and F. Capasso, "A broadband achromatic polarization-insensitive metalens consisting of anisotropic nanostructures," *Nat. Commun.* **10**, 355 (2019).

<sup>7</sup> J. Burch and A. Di Falco, "Surface topology specific metasurface holograms," *ACS Photon.* **5**, 1762-1766 (2018).

<sup>8</sup> G. Zheng, H. Mhlenbernd, M. Kenney, G. Li, T. Zentgraf, and S. Zhang, "Metasurface holograms reaching 80% efficiency," *Nat. Nanotechnol.* **10**, 308-312 (2015).

- <sup>9</sup> X. Ni, A. V. Kildishev, and V. M. Shalaev, “Metasurface holograms for visible light,” *Nat. Commun.* **4**, 2807 (2013).
- <sup>10</sup> B. Wang, F. Dong, Q. Li, D. Yang, C. Sun, J. Chen, Z. Song, L. Xu, W. Chu, Y. Xiao, Q. Gong, and Y. Li, “Visible-frequency dielectric metasurfaces for multiwavelength achromatic and highly dispersive holograms,” *Nano Lett.* **16**, 5235-5240 (2016).
- <sup>11</sup> G. Yoon, D. Lee, K. T. Nam, and J. Rho, “Crypto-display in dual-mode metasurfaces by simultaneous control of phase and spectral responses,” *ACS Nano* **12**, 6421-6428 (2018).
- <sup>12</sup> J. Li, S. Kamin, G. Zheng, F. Neubrech, S. Zhang, and N. Liu, “Addressable metasurfaces for dynamic holography and optical information encryption,” *Sci. Adv.* **4**, 6768 (2018).
- <sup>13</sup> F. Cheng, J. Gao, T. S. Luk, and X. Yang, “Structural color printing based on plasmonic metasurfaces of perfect light absorption,” *Sci. Rep.* **5**, 11045 (2015).
- <sup>14</sup> E. Almpanis and N. Papanikolaou, “Designing photonic structures of nanosphere arrays on reflectors for total absorption” *J. Appl. Phys.* **114**, 083106 (2013).
- <sup>15</sup> E. Almpanis and N. Papanikolaou, “Comparison of Ag and Si nanoparticle arrays: mimicking subwavelength plasmonic field concentrations with dielectric components,” *J. Opt. Soc. Am. B* **33**, 99-104 (2016).
- <sup>16</sup> A. Arbabi, Y. Horie, M. Bagheri, and A. Faraon, “Dielectric metasurfaces for complete control of phase and polarization with subwavelength spatial resolution and high transmission,” *Nat. Nanotechnol.* **10**, 937-943 (2015).
- <sup>17</sup> E. Almpanis, P. A. Pantazopoulos, N. Papanikolaou, V. Yannopapas, and N. Stefanou, “Metal-nanoparticle arrays on a magnetic garnet film for tunable plasmon-enhanced Faraday rotation,” *J. Opt. Soc. Am. B* **33**, 2609-2616 (2016).
- <sup>18</sup> A. Christofi, Y. Kawaguchi, A. Alù, and A. B. Khanikaev, “Giant enhancement of Faraday rotation due to electromagnetically induced transparency in all-dielectric magneto-optical metasurfaces,” *Opt. Lett.* **43**, 1838-1841 (2018).
- <sup>19</sup> T. Stav, A. Faerman, E. Maguid, D. Oren, V. Kleiner, E. Hasman, and M. Segev, “Quantum entanglement of the spin and orbital angular momentum of photons using metamaterials,” *Science* **361**, 1101-1104 (2018).
- <sup>20</sup> S. Chen, G. Li, K. W. Cheah, T. Zentgraf, and S. Zhang, “Controlling the phase of optical nonlinearity with plasmonic metasurfaces,” *Nanophotonics* **7**, 1013-1024 (2018).
- <sup>21</sup> S. Keren-Zur, L. Michaeli, H. Suchowski, and T. Ellenbogen, “Shaping light with nonlinear

- metasurfaces,” *Adv. Opt. Photonics* **10**, 309-353 (2018).
- <sup>22</sup> N. Yu, P. Genevet, M. A. Kats, F. Aieta, J. P. Tetienne, F. Capasso, and Z. Gaburro, “Light propagation with phase discontinuities: generalized laws of reflection and refraction,” *Science* **334**, 333-337 (2011).
- <sup>23</sup> F. Aieta, P. Genevet, N. Yu, M. A. Kats, Z. Gaburro, and F. Capasso, “Out-of-plane reflection and refraction of light by anisotropic optical antenna metasurfaces with phase discontinuities,” *Nano Lett.* **12**, 1702-1706 (2012).
- <sup>24</sup> M. I. Shalaev, J. Sun, A. Tsukernik, A. Pandey, K. Nikolskiy, and N. M. Litchinitser, “High-efficiency all-dielectric metasurfaces for ultracompact beam manipulation in transmission mode,” *Nano Lett.* **15**, 6261-6266 (2015).
- <sup>25</sup> H. Chen, A. J. Taylor, and N. Yu, “A review of metasurfaces: Physics and applications,” *Rep. Prog. Phys.* **79**, 076401 (2016).
- <sup>26</sup> A. Epstein and G. V. Eleftheriades, “Huygens metasurfaces via the equivalence principle: design and applications,” *J. Opt. Soc. Am. B* **33**, A31-A50 (2016).
- <sup>27</sup> C. Pfeiffer and A. Grbic, “Metamaterial Huygens surfaces: Tailoring wave fronts with reflectionless sheets,” *Phys. Rev. Lett.* **110**, 197401 (2013).
- <sup>28</sup> M. Decker, I. Staude, M. Falkner, J. Dominguez, D. N. Neshev, I. Brener, T. Pertsch, and Y. S. Kivshar, “High-efficiency dielectric Huygens surfaces,” *Adv. Opt. Mater.* **3**, 813-820 (2015).
- <sup>29</sup> A. Arbabi, Y. Horie, A. J. Ball, M. Bagheri, and A. Faraon, “Subwavelength-thick lenses with high numerical apertures and large efficiency based on high-contrast transmitarrays,” *Nat. Commun.* **6**, 7069 (2015).
- <sup>30</sup> V. S. Asadchy, M. Albooyeh, S. N. Tsvetkova, A. Daz-Rubio, Y. Ra’di, and S. A. Tretyakov, “Perfect control of reflection and refraction using spatially dispersive metasurfaces,” *Phys. Rev. B* **94**, 075142 (2016).
- <sup>31</sup> N. M. Estakhri and A. Alù, “Wave-front transformation with gradient metasurfaces,” *Phys. Rev. X* **6**, 041008 (2016).
- <sup>32</sup> N. M. Estakhri and A. Al, “Recent progress in gradient metasurfaces,” *J. Opt. Soc. Am. B* **33**, A21 (2016).
- <sup>33</sup> F. Monticone, N. M. Estakhri, and A. Al, “Full control of nanoscale optical transmission with a composite metascreen” *Phys. Rev. Lett.* **110**, 203903 (2013).
- <sup>34</sup> Y. Radi, D. L. Sounas, and A. Al “Metagratings: Beyond the limits of graded metasurfaces for

- wave front control,” *Phys. Rev. Lett.* **119**, 067404 (2017).
- <sup>35</sup> M. Khorasaninejad and F. Capasso, “Broadband multifunctional efficient meta-gratings based on dielectric waveguide phase shifters,” *Nano Lett.* **15**, 6709-6715 (2015).
- <sup>36</sup> Z. Li, E. Palacios, S. Butun, and K. Aydin, “Visible-frequency metasurfaces for broadband anomalous reflection and high-efficiency spectrum splitting,” *Nano Lett.* **15**, 1615-1621 (2015).
- <sup>37</sup> D. Sell, J. Yang, S. Doshay, R. Yang, and J. A. Fan, “Large-angle, multifunctional metagratings based on freeform multimode geometries,” *Nano Lett.* **17**, 3752-3757 (2017).
- <sup>38</sup> R. Paniagua-Domnguez, Y. F. Yu, E. Khaidarov, S. Choi, V. Leong, R. M. Bakker, X. Liang, Y. H. Fu, V. Valuckas, L. A. Krivitsky, and A. I. Kuznetsov, “A metalens with a near-unity numerical aperture,” *Nano Lett.* **18**, 2124-2132 (2018).
- <sup>39</sup> E. Khaidarov, H. Hao, R. Paniagua-Domnguez, Y. F. Yu, Y. H. Fu, V. Valuckas, S. L. K. Yap, Y. T. Toh, J. S. K. Ng, and A. I. Kuznetsov, “Asymmetric nanoantennas for ultrahigh angle broadband visible light bending,” *Nano Lett.* **17**, 6267-6272 (2017).
- <sup>40</sup> Z. Fan, M. R. Shcherbakov, M. Allen, J. Allen, B. Wenner, and G. Shvets, “Perfect diffraction with multi-resonant bianisotropic metagratings,” *ACS Photon.* **5**, 4303-4311 (2018).
- <sup>41</sup> X. M. Zhang, Q. Zhang, S. J. Zeng, Z. Z. Liu, and J. Xiao, “Dual-band unidirectional forward scattering with all-dielectric hollow nanodisk in the visible,” *Opt. Lett.* **43**, 1275-1278 (2018).
- <sup>42</sup> P. Albella, T. Shibanuma, and S. A. Maier, “Switchable directional scattering of electromagnetic radiation with subwavelength asymmetric silicon dimers,” *Sci. Rep.* **5**, 18322 (2015).
- <sup>43</sup> T. Shibanuma, P. Albella, and S. A. Maier, “Unidirectional light scattering with high efficiency at optical frequencies based on low-loss dielectric nanoantennas,” *Nanoscale* **8**, 14184-14192 (2016).
- <sup>44</sup> J. H. Yan, P. Liu, Z. Y. Lin, H. Wang, H. J. Chen, C. X. Wang, and G. W. Yang, “Magnetically induced forward scattering at visible wavelengths in silicon nanosphere oligomers,” *Nat. Commun.* **6**, 7042 (2015).
- <sup>45</sup> W. Liu and Y. S. Kivshar, “Generalized Kerker effects in nanophotonics and meta-optics,” *Opt. Express* **26**, 13085-13105 (2018).
- <sup>46</sup> U. Zywiets, M. K. Schmidt, A. B. Evlyukhin, C. Reinhardt, J. Aizpurua, and B. N. Chichkov, “Electromagnetic resonances of silicon nanoparticle dimers in the visible,” *ACS Photon.* **2**, 913-920 (2015).
- <sup>47</sup> P. Albella, M. A. Poyli, M. K. Schmidt, S. A. Maier, F. Moreno, J. J. Senz, and J. Aizpurua,

- “Low-loss electric and magnetic field-enhanced spectroscopy with subwavelength silicon dimers,” *Phys. Chem. C* **117**, 13573-13584 (2013).
- <sup>48</sup> T. Shibanuma, S. A. Maier, and P. Albella, “Polarization control of high transmission/reflection switching by all-dielectric metasurfaces,” *Appl. Phys. Lett.* **112**, 063103 (2018).
- <sup>49</sup> J. Q. Li, N. Verellen, and P. Van Dorpe, “Engineering electric and magnetic dipole coupling in arrays of dielectric nanoparticles,” *J. Appl. Phys.* **123**, 083101 (2018).
- <sup>50</sup> S. Inampudi and H. Mosallaei, “Neural network based design of metagratings,” *Appl. Phys. Lett.* **112**, 241102 (2018).
- <sup>51</sup> N. Stefanou, V. Yannopoulos, and A. Modinos, “Heterostructures of photonic crystals: frequency bands and transmission coefficients,” *Comput. Phys. Commun.* **113**, 49-77 (1998).
- <sup>52</sup> N. Stefanou, V. Yannopoulos, and A. Modinos, “MULTEM 2: A new version of the program for transmission and band-structure calculations of photonic crystals,” *Comput. Phys. Commun.* **132**, 189-196 (2000).
- <sup>53</sup> G. Gantzounis and N. Stefanou, “Layer-multiple-scattering method for photonic crystals of nonspherical particles,” *Phys. Rev. B* **73**, 035115 (2006).
- <sup>54</sup> J. M. MacLaren, S. Crampin, D. D. Vvedensky, R. C. Albers, and J. B. Pendry, “Layer Kohn-Rostoker electronic structure code for bulk and interface geometries,” *Comput. Phys. Commun.* **60**, 365-389 (1990).
- <sup>55</sup> J. M. Geffrin, B. Garcia-Cmara, R. Gmez-Medina, P. Albella, L. S. Froufe-Prez, C. Eyraud, A. Litman, R. Vaillon, F. Gonzalez, M. Nieto-Vesperinas, J. J. Senz, and F. Moreno, “Magnetic and electric coherence in forward- and back-scattered electromagnetic waves by a single dielectric subwavelength sphere,” *Nat. Commun.* **3**, 1171 (2012).
- <sup>56</sup> H. Y. Fu, A. I. Kuznetsov, A. E. Miroshnichenko, Y. F. Yu, B. Lukyanchuk, “Directional visible light scattering by silicon nanoparticles,” *Nat. Commun.* **4**, 1527 (2013).
- <sup>57</sup> M. I. Tribelsky, J. M. Geffrin, A. Litman, C. Eyraud, and F. Moreno, “Small dielectric spheres with high refractive index as new multifunctional elements for optical devices,” *Sci. Rep.* **5**, 12288 (2015).
- <sup>58</sup> A. Mirzaei, A. E. Miroshnichenko, “Electric and magnetic hotspots in dielectric nanowire dimers,” *Nanoscale* **7**, 5963-5968 (2015).
- <sup>59</sup> V. E. Babicheva, M. I. Petrov, K. V. Baryshnikova, and P. A. Belov, “Reflection compensation mediated by electric and magnetic resonances of all-dielectric metasurfaces,” *J. Opt. Soc. Am.*

- B **34**, D18-D28 (2017).
- <sup>60</sup> B. Slovick, Z. G. Yu, M. Berding, and S. Krishnamurthy, “Perfect dielectric-metamaterial reflector,” *Phys. Rev. B* **88**, 165116 (2013).
- <sup>61</sup> H. Chalabi, Y. Radi, D. L. Sounas, and A. Al, “Efficient anomalous reflection through near-field interactions in metasurfaces,” *Phys. Rev. B* **96**, 075432 (2017).
- <sup>62</sup> W. Liu, “Generalized magnetic mirrors,” *Phys. Rev. Lett.* **119**, 123902 (2017).
- <sup>63</sup> Y. F. Yu, A. Y. Zhu, R. Paniagua-Domnguez, Y. H. Fu, B. Lukyanchuk, and A. I. Kuznetsov, “High-transmission dielectric metasurface with  $2\pi$  phase control at visible wavelengths,” *Laser Photon. Rev.* **9**, 412418 (2015).
- <sup>64</sup> R. Paniagua-Domnguez, Y. F. Yu, E. Khaidarov, S. Choi, V. Leong, R. M. Bakker, X. Liang, Y. H. Fu, V. Valuckas, L. A. Krivitsky, and A. I. Kuznetsov, “A metalens with a near-unity numerical aperture,” *Nano Lett.* **18**, 21242132 (2018).
- <sup>65</sup> D. E. Aspnes, Properties of silicon, in *EMIS Datareviews* (Inspec IEE, 1988).
- <sup>66</sup> For a Si sphere in air the dipolar magnetic Mie mode is found at  $\lambda_{DM} \approx 900$  nm and the dipolar electric at  $\lambda_{DE} \approx 700$  nm, while the magnetic quadrupole resonance is close to  $\lambda_{QM} \approx 660$  nm.
- <sup>67</sup> Y. H. Ko and R. Magnusson, “Wideband dielectric metamaterial reflectors: Mie scattering or leaky Bloch mode resonance?,” *Optica* **5**, 289-294 (2018).
- <sup>68</sup> F. Monticone and A. Alù, “Bound states within the radiation continuum in diffraction gratings and the role of leaky modes,” *New J. Phys.* **19**, 093011 (2017).
- <sup>69</sup> C. Blanchard, J. P. Hugonin, and C. Sauvan, “Fano resonances in photonic crystal slabs near optical bound states in the continuum,” *Phys. Rev. B* **94**, 155303 (2016).